

Photosynthetic performance of benthic microbial mats in Lake Hoare, Antarctica

Kay Vopel¹

National Institute of Water and Atmospheric Research, P.O. Box 11-115, Hamilton, New Zealand

Ian Hawes

World Fish Center, Nusa Tupe, P.O. Box 77, Western Province, Solomon Islands

Abstract

We measured in situ photosynthesis of benthic microbial mats at various depths in Lake Hoare, a permanently ice-covered lake of the McMurdo Dry Valleys, Antarctica, using oxygen (O₂) microelectrodes. We further investigated the vertical distribution and activity of pigments in the microbial mats using an imaging pulse-amplitude-modulated fluorometer. Microbial mats to at least 16.6-m water depth are net producers of O₂ during the summer period. Net O₂ production ranges from 100–500 $\mu\text{mol m}^{-2} \text{h}^{-1}$ at incident downwelling irradiances of photosynthetically active radiation (PAR) of 1.0–4.6 $\mu\text{mol quanta m}^{-2} \text{s}^{-1}$. Photosynthesis of mat-forming cyanobacteria and diatoms occurs at all lake depths at or close to maximum efficiency. We measured absorption by the pigment arrays at a single water depth and, by assuming that absorption is water-depth invariant, we estimated an area-specific maximum community quantum yield of 0.073 mol carbon per mol photons. A community compensation irradiance of 0.1 $\mu\text{mol quanta m}^{-2} \text{s}^{-1}$ was estimated, reflecting extreme shade acclimation. These results confirm estimates previously derived from laboratory gas-exchange measurements and imply that even minor changes in the intensity of the incident downwelling irradiance of PAR caused by, for example, changes in the transparency of the ice cover or the optical properties of the water column can significantly alter rates of benthic carbon fixation. In situ measurements were confined to mats with flat surfaces. Laboratory measurements at the surface of mats with pinnacled surfaces revealed a complex small-scale chemical structure at the mat–water interface.

The largest ice-free region of Antarctica, the Dry Valley Region of Southern Victoria Land, is among the coldest and driest deserts in the world (Heywood 1984). The dry valley mean annual temperature ranges from -14.8°C to -30.0°C (Doran et al. 2002a). The low mean annual temperature allows perennial, 3–6-m-thick ice covers to persist on numerous meltwater lakes in the valley systems. The ice covers have profound effects on these lakes: they eliminate turbulent mixing of the water column by wind-generated currents, reduce light penetration, and restrict gas exchange between the atmosphere and the water column. Among the unique features of these lakes that have developed as a consequence of ice cover is the oxygen (O₂) supersaturation of the water column (Parker et al. 1981; Craig et al. 1992). A second unusual feature is the occurrence of modern and nascent stromatolites: laminated photosynthetic communities, dominated by cyanobacteria, which cover much of the lake floors (Wharton et al. 1983; Hawes and Schwarz 1999).

Whereas numerous studies of photosynthetic production in the dry valley lakes have focused on planktonic

microbial communities (e.g., Vincent 1981; Priscu et al. 1987; Dore and Priscu 2001), few studies have dealt with benthic communities (Wharton et al. 1994; Hawes and Schwarz 1999, 2000; Wharton et al. 2001). The study of Wharton et al. (1994) revealed evidence for benthic photosynthesis. These authors found significant differences in pore water [O₂] profiles measured in sediment cores taken from Lake Hoare in January and October; they suggested that this difference is due to a seasonal cycle resulting from the long photoperiod and photosynthesis by mat-forming benthic microbial communities. Subsequent laboratory gas-exchange measurements demonstrated that mats taken in Lake Hoare from water depths of up to 22 m are capable of photosynthesizing at the low irradiance they would experience under ambient conditions (Hawes and Schwarz 1999, 2000). Hawes and Schwarz (1999) suggested that, in this diffusion-dominated lake, benthic biomass accumulation is favored by retention of nutrients in close proximity to growing cells, with minimal expenditure of energy in swimming or loss to grazers. In a modeling exercise, Hawes et al. (2001) then used their experimentally derived observations of mat photosynthesis and respiration, with data on incident downwelling irradiance of photosynthetically active radiation (PAR; see Table 1) and the optical properties of the ice and water column (Howard-Williams et al. 1998), to predict net photosynthetic production from October to February, net respiration at other times, and a maximum annual rate of carbon fixation of 12 g carbon m⁻², equating to approximately 0.1–4-mm vertical accumulation of mat each year. Finally, using the experimental observations of Hawes and Schwarz (1999, 2000) and a mathematical model, Moorhead et al.

¹ Corresponding author (k.vopel@niwa.co.nz).

Acknowledgments

R. Ellwood assisted in the field. Two anonymous reviewers, the Associate Editor R. N. Glud, P. Doran, C. Howard-Williams, J. Meadows, and A. Vopel commented on an earlier draft.

The New Zealand Foundation for Research, Science and Technology (CO1605), Antarctica New Zealand, and the McMurdo Dry Valley Long Term Ecological Research Program of the U.S. National Science Foundation (OPP-9814972) funded and provided facilities and support for the research.

Table 1. Abbreviations.

Symbol	Definition
ϕ	Mat porosity
ϕ_p	Quantum yield of charge separation in photosystem complex II
ΔF	Variable fluorescence (the difference between F_0 and F_m or F and F'_m)
AOI	Area of interest
D_0	Free-solution diffusion coefficient ($\text{cm}^2 \text{s}^{-1}$)
DBL	Diffusive boundary layer
D_S	Sediment diffusion coefficient ($\text{cm}^2 \text{s}^{-1}$)
E_d	Incident downwelling irradiance of photosynthetically active radiation ($\text{mol quanta m}^{-2} \text{s}^{-1}$)
E_k	Irradiance above which photosynthesis is light saturated ($\text{mol quanta m}^{-2} \text{s}^{-1}$)
ETR	Rate of photosynthetic electron transport between photosystem complex II and I ($\text{mol electrons m}^{-2} \text{s}^{-1}$)
F	Current fluorescence yield of light-adapted sample
F_0, F_m	Minimal and maximal fluorescence yield of dark-adapted sample, respectively
F'_m	Maximal fluorescence yield of light-adapted sample
J	Diffusive flux of O_2 ($\text{mol m}^{-2} \text{h}^{-1}$)
K_L	Diffuse attenuation coefficient of scalar irradiance (mm^{-1})
LED	Light-emitting diode
PAR	Photosynthetically active radiation ($\text{mol quanta m}^{-2} \text{s}^{-1}$)
PSI and PSII	Photosystem complex I and II
rETR _{max}	Maximum relative rate of photosynthetic electron transport between photosystem complex II and I ($\text{mol electrons m}^{-2} \text{s}^{-1}$)
RLC	Rapid light curve
A	Slope of irradiance versus rETR as irradiance approaches zero ($[\text{mol electrons m}^{-2} \text{s}^{-1}] \times [\text{mol quanta m}^{-2} \text{s}^{-1}]^{-1}$)
σ_a	Absorption cross section of photosystem complex II

(2005) simulated whole-lake, annual net primary production of benthic microbial mats in Lake Hoare and compared these estimates to observed phytoplankton production. These authors suggested that benthic microbial mats have the capacity to fix quantities of carbon that rival or exceed carbon fixation by planktonic communities; on average, simulated benthic mat production represented >85% of the combined benthic and planktonic carbon fixation.

Moorhead et al. (2005) noted that 79–99% of the uncertainty in the behavior of their model was attributed to uncertainties in estimates of the maximum photosynthetic rate, the initial slope of photosynthetic-light response, and the maximum respiration rate. These parameters were estimated from measurements of the rate of evolution or consumption of O_2 in laboratory mat enclosures (Hawes and Schwarz 1999). Hawes and Schwarz (1999) discussed the limitations of this method and noted methodological necessities that may have altered the nutrient supply of the mats and the mat–water O_2 exchange. For example, incubating mat explants altered the thickness of the diffusive boundary layer (DBL) between the mat surface and the overlying lake water and enabled solute exchange across the cut side and bottom of the cores, which would not occur naturally. Thus, the photosynthetic parameters require confirmation under in situ conditions.

The aims of this study are to estimate in situ, for the first time, the magnitude of benthic photosynthesis in a permanently ice-covered lake of the McMurdo Dry Valleys, to reassess photosynthetic parameters, and to resolve benthic photosynthesis vertically. To do so, we measured, with the aid of surface-air-supply diving, O_2 microprofiles across the

mat–water interface at various depths in Lake Hoare. To obtain supplement data to help interpret O_2 microprofiles, we investigated mat cross sections in the laboratory using an imaging pulse-amplitude-modulated fluorometer (Imaging-PAM).

Material and methods

Study site—Lake Hoare ($77^\circ 38' \text{S}$, $162^\circ 53' \text{E}$) is a closed-basin lake near the eastern end of Taylor Valley in southern Victoria Land, Antarctica. The lake is 4.2-km long and 1-km wide, and has maximum and mean depths of 34 m and 14 m. Lake Hoare is dammed to the northeast by the Canada Glacier, which provides an inflow of glacial meltwater. Other inflow comes from Andersen Creek entering the northeast corner of Lake Hoare, and drainage is from Lake Chad in the southeast. No outflows from Lake Hoare exist, so water loss is restricted to sublimation of ice and evaporation of meltwater during summer. The average mean annual temperature at Lake Hoare between 1985 and 2000 was -17.7°C (Doran et al. 2002a). The ice cover of this lake is perennial, except for small areas at the lake margin that melt during most summers. The thickness of the ice cover was 3.5 m in 1983 (Wharton et al. 1993), ~ 5 m in 2002 (Doran et al. 2002b), and < 4 m in 2004. There are 3 months of complete darkness during winter and 3 months of continuous light during summer. Net transmission of solar radiation through the ice cover is $< 1\text{--}3\%$, with a spectral transmission peak at wave lengths of 450–550 nm. Vertical extinction coefficients for PAR within the water column from beneath the ice to a depth of 33 m were typically $0.12\text{--}0.22 \text{ m}^{-1}$ (Howard-Williams et al. 1998). The lake has a density-stabilized water column, with

a pronounced inflection in the density–depth profile at 13–15 m from the surface (the depth of the lake varies temporally), which divides the lake into upper and lower compartments. The upper compartment is characterized by lower concentrations of dissolved nutrients, particularly nitrate (Lizotte and Priscu 1992), higher concentrations of O_2 ($0.94\text{--}1.25\text{ mmol L}^{-1}$ compared to $0.63\text{--}0.94\text{ mmol L}^{-1}$ below, Wharton et al. 1986), lower bicarbonate, and higher pH (up to 8.6 compared to 7.9 below, Cathey et al. 1981). The lake is anoxic below 25–26 m depth.

Benthic microbial mats—Benthic microbial mats in different zones of Lake Hoare differ in structure and species composition; the quantity and quality of the incident downwelling irradiance of PAR are apparently the most important factors that regulate these differences (Wharton et al. 1983). Three mat morphologies are common: moat mats, columnar lift-off mats, and prostrate mats; the surface of the last can be smooth (Fig. 1A) but surface irregularities can occur in the form of pinnacles up to 3-cm high (Fig. 1B). Columnar lift-off mats and prostrate mats comprise a matrix of filamentous cyanobacteria and pennate diatoms, whereas moat mats are dominated by cyanobacteria (Wharton et al. 1983). Lift-off mats occur in shallow under-ice environments, where both N_2 and O_2 approach their saturation concentrations. Gas ebullition within lift-off mats makes them buoyant; hence they lift away from the underlying sediment until they rise up and freeze into the ice (Wharton et al. 1986). Prostrate mats occur in deeper water where gas ebullition does not occur. Moat mats, which freeze solid during winter and experience high quantities of incident downwelling irradiance of PAR during the brief ice-free period in summer, are different than the other types; they are <3-cm thick, weakly stratified, and have smooth surfaces that follow the contours of underlying sediments and rocks.

In situ measurements—In November 2004, a surface-supplied tethered diver measured a total of 10 in situ high-resolution $[O_2]$ profiles across the mat–water interface at four depths along a transect away from a 1-m diameter hole melted through the ice (Table 2). The profiles were measured in areas devoid of pinnacles (e.g., see Fig. 1A). To do so, the diver attached a Clark-type underwater O_2 microelectrode (Revsbech 1989, Unisense) to a manually operated micromanipulator (Märzhäuser Wetzlar) mounted on an aluminum post that had been driven into the lake sediment. An underwater picoammeter PA 3000U (Unisense) placed onto the sediment surface provided the polarization voltage for the O_2 microelectrode, which had an outside tip diameter of $50\ \mu\text{m}$, a 90% response time of $\sim 1\text{ s}$, and a stirring sensitivity of $<2\%$. The diver used the micromanipulator to move the electrode in 0.2-mm increments normal to the mat surface from a position above the DBL to a depth of 6–7 mm into the mat and further in 0.5-mm increments to a maximum depth of 21 mm. After each depth interval the diver verbally relayed the electrode reading to the support person at the surface of the ice, who recorded the data.

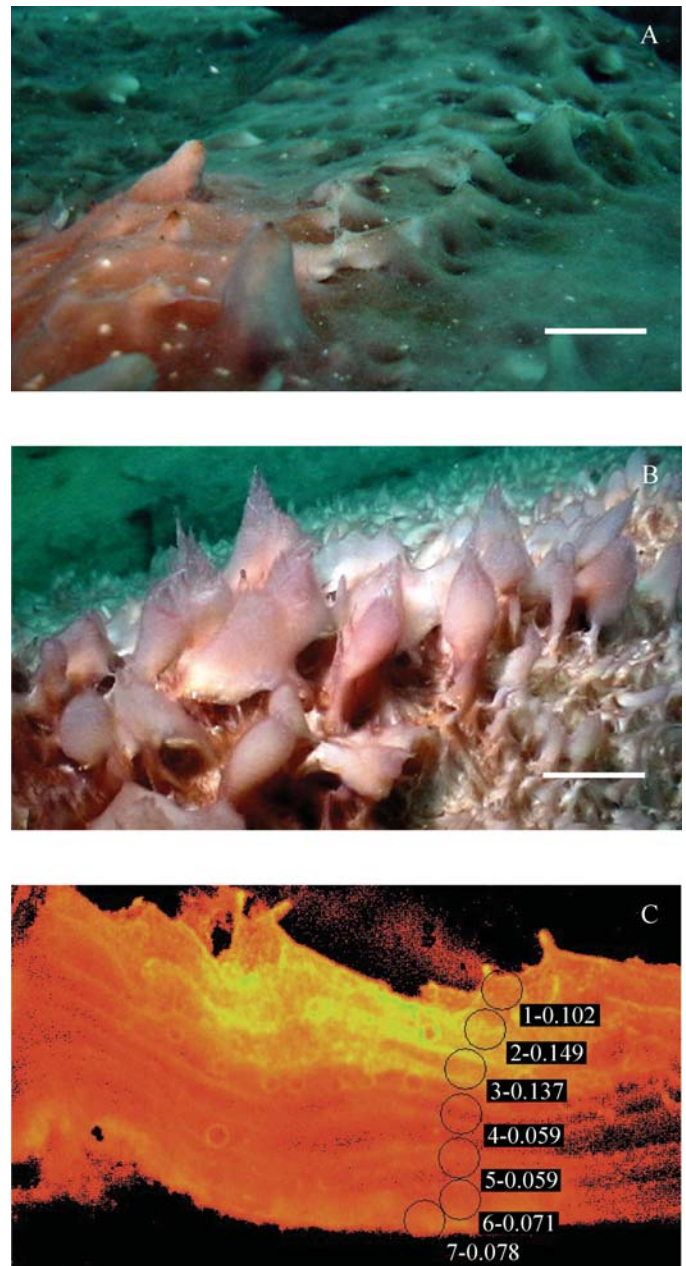


Fig. 1. (A, B) Underwater photographs of prostrate microbial mats at $\sim 8\text{-m}$ water depth. The surface of the mats can be (A) smooth or (B) structured by pinnacles. Scale bars, 10 mm, apply to the center of the photograph. (C) Chlorophyll fluorescence image of a mat cross section. Areas of interest (AOI) were defined to provide a continuous vertical transect through the cross section.

We determined the downwelling irradiance of PAR incident to the surface of the microbial mat once before every in situ profiling measurement using a newly calibrated LI-COR LI 192 underwater quantum sensor and LI-189 light meter in a waterproof housing. A StowAway Tidbit miniature temperature data logger (Onset Computer Cooperation) placed onto the surface of a microbial mat at 8-m water depth measured and logged the bottom water temperature once every minute from 18 to 24 November 2004.

Table 2. In situ profiling along a depth profile away from the ice hole.

Date	Depth (m)	PAR ($\mu\text{mol quanta m}^{-2} \text{ s}^{-1}$)	Number of profiles
21 Nov 2004	8.1	4.6	4
22 Nov 2004	9.2	3.5	2
23 Nov 2004	16.3	2.2	2
24 Nov 2004	16.6	1.0	2

To estimate the mean spectral transmission of the ice cover, on 22 November 2004 we measured spectra immediately beneath the ice at seven random points, all well clear of the anomalous light field close to the dive hole, using a hyperspectral irradiance sensor (RAMSES-ACC-UV/VIS, TriOS). The diver then deployed the sensor at 4 m, 7 m, 10 m, and 13 m below the ice cover for estimation of spectral attenuation coefficients for downwelling irradiance by log-linear regression of irradiance-versus-depth profiles.

Sampling—To collect mats the diver cut a random series of core samples, 10 cm in diameter by 3-cm deep, of the “active layer” (*sensu* Hawes and Schwarz 1999) of microbial mats from within 3-m-diameter sampling areas, at water depths ranging from 8–16 m. These discs were carefully separated from underlying materials and transferred into an opaque polyethylene box with a watertight sealed lid. Additionally, five 150-mL water samples were collected from ~3 cm above the surface of the microbial mats at water depths of 5 m, 8 m, 12 m, and 16 m, and underwater photographs of the mat surface were taken using a Sony Cyber-shot DSCP-8 digital camera. The mat and water samples were moved to a dark tent-laboratory next to the ice hole for chemical analyses or to a lakeside laboratory for fluorescence measurements (*see* below).

Laboratory measurements—Salinity, pH, and $[\text{O}_2]$ of the bottom water were measured with two PortaMess 913 meters, the picoammeter PA 3000U, the conductivity sensor SE 204, the pH/Pt1000 electrode SE 102 (Knick), and a Clarke-type O_2 microelectrode. Thereafter the O_2 microelectrode was mounted on a motorized micromanipulator attached to a stand to record three $[\text{O}_2]$ microprofiles across the mat–water interface of a pinnacle mat from 12-m water depth at 200- μm resolution. The mat was fixed at the bottom of the sampling box to ensure a constant distance between micromanipulator and mat. Pieces of ice were added to the water surrounding the mat to control temperature. The profiles were measured vertically and normal to the mat surface starting at different vertical distances from a fixed position in the overlying water. The position of the mat surface was determined visually as the depth at which the tip of the microelectrode first penetrated the mat. The PC Windows program PROFIX (Unisense) controlled the stepwise movement of the micromanipulator via a motor controller and read the data from the microsensor amplifiers via an A/D converter (ADC-216USB, Unisense) that was connected to the parallel port

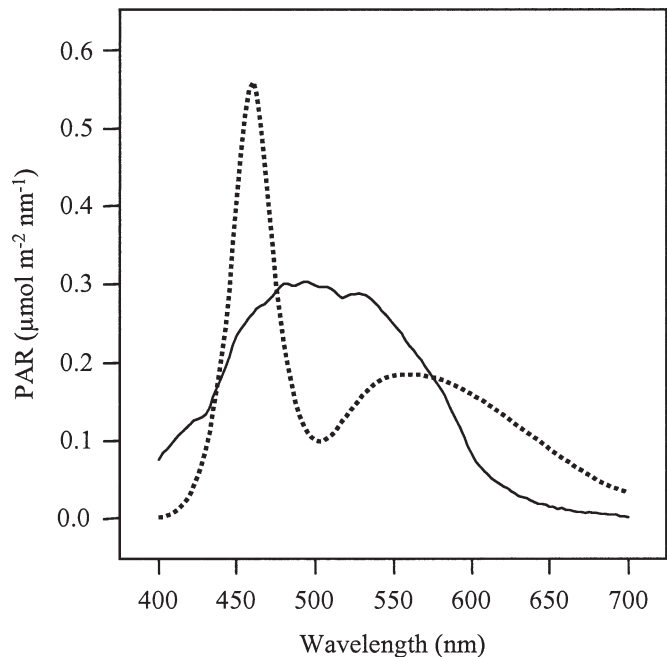


Fig. 2. Under-ice PAR spectrum (solid line) and spectrum of LED light source (dotted line).

of a personal computer. The O_2 microelectrode was calibrated in 100% air-saturated lake water and in lake water that had been deoxygenated with sodium sulfite.

Appropriate levels of PAR were supplied to the surface of the mat with battery-powered light-emitting diode (LED) at a previously determined distance from the surface. This distance was determined by measuring the downwelling irradiance of PAR supplied by the LED to a quantum sensor in a water-filled plastic tube so that 5 cm of water were above the sensor head. The spectrum of this irradiance was measured by submerging the hyperspectral irradiance sensor in lake water and clamping it in place a similar distance from the LED source to that used during profiling measurements. The spectrum of the under-ice downwelling irradiance of PAR was compared with that of the LED by calculating the spectrum of downwelling irradiance of PAR for 8-m water depth from ice transmission and water-column attenuation. The under-ice spectrum was dominated by a single peak spanning wavelengths of 450–570 nm. The spectrum of the LED showed two peaks within this range, at 460 nm and 560 nm, although both spectra tailed off above 600 nm (Fig. 2).

The attenuation of scalar irradiance through a microbial mat from 8-m water depth was measured by means of a scalar fiber-optic microprobe connected to a spectrometer (S2000, Ocean Optics) fitted with a diffraction grating that allowed coverage between 350 nm and 850 nm. The microprobe was constructed following Lassen et al. (1992), and the scalar detector at the tip of the probe had a diameter of 0.3 mm. The probe was inserted into the mat with the micromanipulator at an angle of 15 degrees from vertical. A blue-enhanced quartz-halogen light source provided PAR from above via a fiber-optic bundle. Spectra just above the mat surface, just below the surface, and in 1-

mm increments to a maximal depth of 9 mm were recorded. Data were integrated across four, 10-nm wavebands, 575–585, 625–635, 670–680, and 740–750 nm. The diffuse attenuation coefficient of scalar irradiance in each waveband was calculated as the rate of change of log-transformed irradiance values with depth using $K_L = -d(\ln L) \times dz^{-1}$ (Kirk 1983).

Imaging-PAM (Walz Mess- und Regeltechnik) and the saturation pulse method were used to determine the two-dimensional (horizontal or vertical) distribution and activity of pigments, measuring the minimal (F_0) and maximal (F_m) fluorescence yields of dark-adapted mat samples. For a detailed description of the saturation pulse method see, for example, Schreiber et al. (1996) or Kühl et al. (2001) and literature cited therein. Use of the Imaging-PAM to obtain spatially resolved measures of fluorescence is described by Ralph et al. (2005) and Grunwald and Kühl (2004). Measurements of F_0 were to obtain a proxy for the distribution of chlorophyll. Comparing the distribution of F_0 with that of the maximal photochemical yield, $(F_m - F_0) \times F_m^{-1}$, gave us an index of chlorophyll connectivity to photosystem complex II (PSII) electron transport chains. The primary goal of F_m measurements was to determine whether F_0 was attributable to pigments connected to competent electron transport systems. The Imaging-PAM output these two parameters as false-color images that could then be compared with photographic images of the same section.

The Imaging-PAM was set up to image an area of 30 mm \times 25 mm. A millimeter scale was imaged at intervals during sampling runs. Using a scalpel, we cut 2–3-mm-thick cross sections, running for the full thickness of the active layer and each approximately 40-mm long, from freshly collected material. These sections were then laid on their sides in a Petri dish and immersed in fresh lake water. At this thickness, the laminations in the mat could be easily seen, while sufficient chlorophyll was still viewed in cross section by the Imaging-PAM to obtain acceptable fluorescence intensities (we aimed for at least 200 fluorescence units across the pigmented areas of the image) and replicable measurements. Actinic light from the Imaging-PAM was provided by a bank of blue-white LEDs. The spectrum of this light has two peaks, at 450 and 550 nm—blue and blue-green. Different absorption spectra for diatoms, which can be expected to show strongest fluorescence in response to the blue peak, and the phycoerythrin-rich cyanobacteria from Lake Hoare, which absorb maximally close to the blue-green peak (Hawes and Schwarz 2000), will result in different fluorescence responses per unit biomass for the two groups of phototrophs. Thus, while F_0 will remain a proxy for chlorophyll fluorescence in the microbial mats, care must be taken in interpreting the false color images.

The Imaging-PAM facility for defining areas of interest (AOIs) was used to provide insight to the photoadapted status of the microbial mats using rapid light curves (RLCs). First we defined AOI to provide a vertical transect through a mat cross section (Fig. 1C). The Imaging-PAM had a restricted spatial resolution when used with AOI; the diameter of the circles in Fig. 1C is \sim 2 mm. The

instrument was therefore best suited to the thicker mats, where the size of AOI was similar to lamina thickness. Accordingly, only RLC data from mats from 12-m depth were reported. RLCs for AOIs were recorded by exposing mat cross sections to a sequence of actinic irradiances in 14 discrete PAR steps from 0 μ mol quanta $m^{-2} s^{-1}$ to 52 μ mol quanta $m^{-2} s^{-1}$. To control for hysteresis effects, the order of PAR was not fully sequential, but ran 0, 3.6, 6.9, 10.9, 3.6, 27.9, 38, 52, 3.6, 27.9, 19, 3.6, 6.8, 0 μ mol quanta $m^{-2} s^{-1}$. In practice, no hysteresis effects were observed. The incident downwelling irradiance of PAR supplied by blue-white LEDs (see above) was measured using a recently calibrated LI-COR 190 quantum sensor connected to a LI-COR Li 1000 digital meter, set to average over 5-s intervals, positioned in place of the Petri dish. Each period of actinic light lasted for 30 s, leading to a quasi-steady-state level of fluorescence, F . This period is longer than is commonly used for RLCs (10–15 s, see e.g., Hawes et al. 2003, Ralph and Gademann 2005). We found that a slightly longer actinic exposure of microbial mats from Lake Hoare produced more repeatable measures of variable fluorescence, ΔF , and the absence of hysteresis effects suggests that this exposure was not affecting the photoadaptive state. At the end of each actinic period, a saturation pulse of white light (0.6 s at $>500 \mu$ mol quanta $m^{-2} s^{-1}$) was applied to determine the maximal fluorescence yield, F'_m , and the quantum yield of charge separation in PSII, $\phi_p = (F'_m - F) \times F'_m^{-1}$. We were unable to measure the intensity of the saturation pulse with the instrumentation available, but preliminary trials were undertaken to ensure that the width and intensity of this saturation pulse was adequate to attain maximum fluorescence yield. The photosynthetic electron transport rate (ETR) between PSII and PSI can be estimated as $ETR = \phi_p \times \sigma_a \times E_d$, where σ_a is the absorption cross section of PSII, and E_d is the incident downwelling irradiance of PAR. Assuming that σ_a is an unknown constant during the measurements, the relative ETR was estimated as $rETR = \phi_p \times E_d$ (Hofstraat et al. 1994). A modification of the Jassby and Platt (1976) equation was used to calculate the irradiance above which photosynthesis is light saturated, E_k , using least-squares regression (SigmaPlot 8.0, SPSS Inc.), as $rETR = rETR_{max} \times \tanh(E_d \times E_k^{-1})$, where $E_k = rETR_{max} \times \alpha^{-1}$ and α is the slope of the light-limited portion of the PAR versus ETR relationship. To avoid biasing the regression, repeat measures of ϕ_p at 3.6 μ mol quanta $m^{-2} s^{-1}$ in the actinic light sequence were excluded.

Analysis of in situ microprofiles—The diffusive flux (J) of O_2 from the microbial mat into the overlying bottom water was calculated from the measured steady-state O_2 gradients ($dC \times dz^{-1}$) in the DBL according to $J = -D_0 dC \times dz^{-1}$, where D_0 is the free-solution diffusion coefficient of O_2 , C is $[O_2]$, and z is depth. Values of D_0 were taken from Broecker and Peng (1974) and were recalculated to the experimental temperature with the Stokes–Einstein relation (Li and Gregory 1974). The position of the mat surface was determined by a break in the $[O_2]$ profile. This inflection is required for mass conservation in the diffusive flux, because of the shift in apparent diffusivity between the

DBL and the matrix of the mat. Vertical zones of metabolic activity were detected with a numerical procedure for the interpretation of steady-state microprofiles (Berg et al. 1998). We used one in situ $[O_2]$ profile measured at 8.1-m and 16.6-m water depth to calculate depth profiles of volumetric net O_2 production rates (unit: $nmol\ cm^{-3}\ s^{-1}$) and area-specific depth-integrated net O_2 production rates for each activity zone and for the upper 21 mm of the mats (unit: $\mu mol\ m^{-2}\ h^{-1}$). Mat porosity, $\phi = 0.80 \pm 0.08$ ($n = 7$), was estimated following the approach described in Epping et al. (1999) assuming the sediment diffusion coefficient $D_S = D_0 (1 + 3 \times (1 - \phi))^{-1}$ and conservation of O_2 flux across the mat-water interface. We assumed ϕ and D_S to be depth invariant.

Results

Bottom water chemistry, attenuation of scalar irradiance within the mat, and benthic production—The bottom water salinity increased with depth from 0.30 ± 0.00 to 0.62 ± 0.04 , whereas the pH decreased from 8.97 ± 0.03 to 7.59 ± 0.09 (Fig. 3A,B). The $[O_2]$ of the bottom water was highest at 8-m depth ($337 \pm 16\%$ saturation) and lowest at 16-m depth ($134 \pm 5\%$ saturation, Fig. 3C). The temperature of the bottom water at 8-m water depth was constant: $0.11^\circ C$.

The diffuse attenuation coefficients of scalar irradiance, K_L , in four 10-nm wavebands (575–585, 625–635, 670–680, and 740–750 nm) were highest just below the surface of a mat from 8-m water depth (4.72, 3.83, 5.54, and $1.59\ mm^{-1}$) and decreased to a minimum at about 1.2-mm depth within the mat (0.005, 0.005, 0.010, and $0.0004\ mm^{-1}$). Further down, K_L increased asymptotically, reaching its maxima at a depth of 4 mm at 0.76, 0.64, and $0.77\ mm^{-1}$ in the 575–585-nm, 625–635-nm, and 670–680-nm wavebands, respectively, and at $0.37\ mm^{-1}$ at wave lengths between 740 nm and 750 nm.

The incident downwelling irradiance of PAR (hereafter irradiance of PAR) reaching microbial mats at water depths of 8.1, 9.2, 16.3, and 16.6 m varied between $1\ \mu mol\ quanta\ m^{-2}\ s^{-1}$ to $5\ \mu mol\ quanta\ m^{-2}\ s^{-1}$ (Table 2). Low irradiance of PAR of $1.0\ \mu mol\ quanta\ m^{-2}\ s^{-1}$ at 16.6-m water depth caused an average O_2 efflux of $93\ \mu mol\ m^{-2}\ h^{-1}$. The efflux increased linearly with irradiance of PAR; the highest average efflux of $482\ \mu mol\ m^{-2}\ h^{-1}$ was calculated from profiles measured at 8.1-m water depth under conditions of irradiance of PAR = $4.6\ \mu mol\ quanta\ m^{-2}\ s^{-1}$ (Fig. 4). Note that estimates of O_2 flux were on the basis of area, integrated across the depth of the photosynthetic active mat plus the underlying organic material, which is different for each water depth.

Analysis of a profile measured across the upper 21 mm of a mat from 8.1-m water depth under conditions of irradiance of PAR = $4.6\ \mu mol\ quanta\ m^{-2}\ s^{-1}$ (Fig. 5A) revealed depth-integrated net O_2 production of $441\ \mu mol\ m^{-2}\ h^{-1}$. Calculation of the O_2 flux across the DBL revealed a similar value of $493\ \mu mol\ m^{-2}\ h^{-1}$. We found three distinct zones of net O_2 production/consumption: high production ($399\ \mu mol\ O_2\ m^{-2}\ h^{-1}$) in the upper 3-mm-thick layer, low production ($93\ \mu mol\ O_2\ m^{-2}\ h^{-1}$)

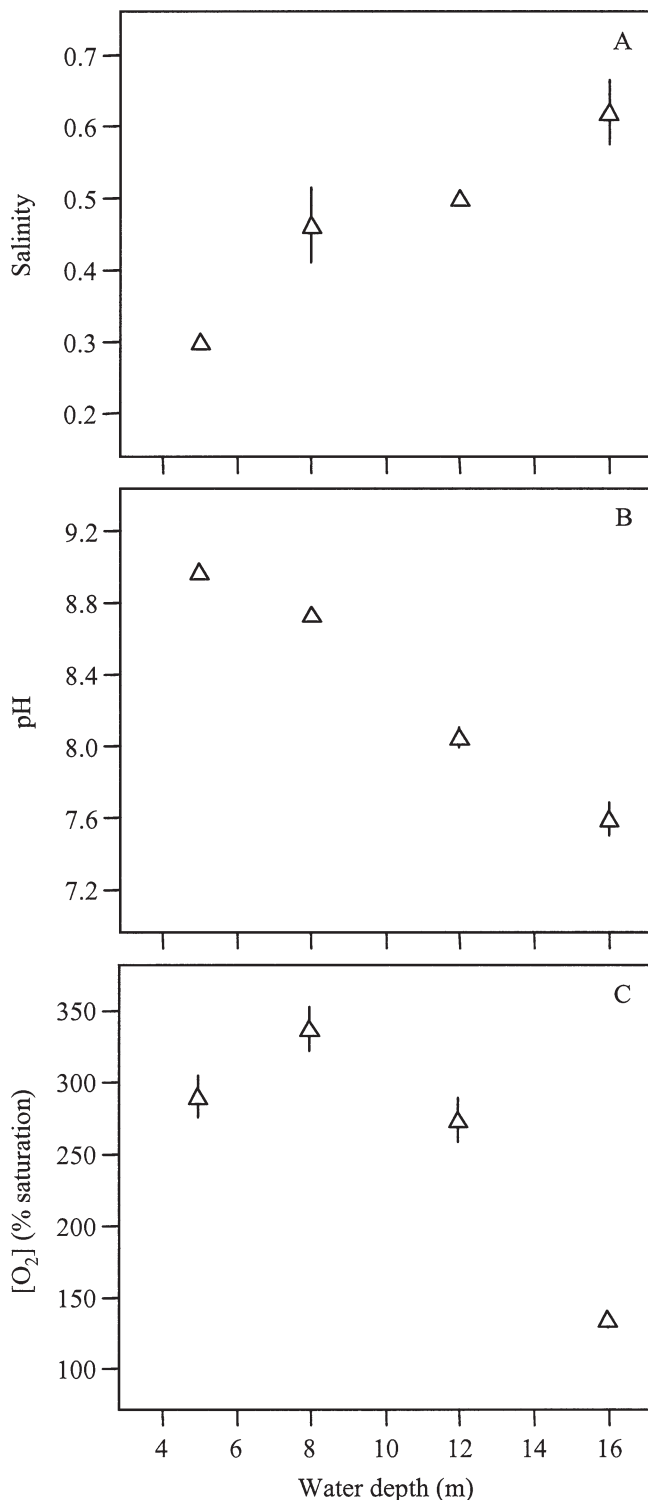


Fig. 3. (A) Bottom-water salinity, (B) pH, and (C) $[O_2]$ measured along a transect from beneath the ice hole to 16-m depth. Symbols indicate the mean ($n = 5$), and vertical lines indicate standard deviations.

between 3-mm and 6-mm depth, and consumption of $51\ \mu mol\ O_2\ m^{-2}\ h^{-1}$ between 6-mm and 21-mm depth. Note that rates in the production profiles shown in Fig. 5 are given per volume of mat/sediment.

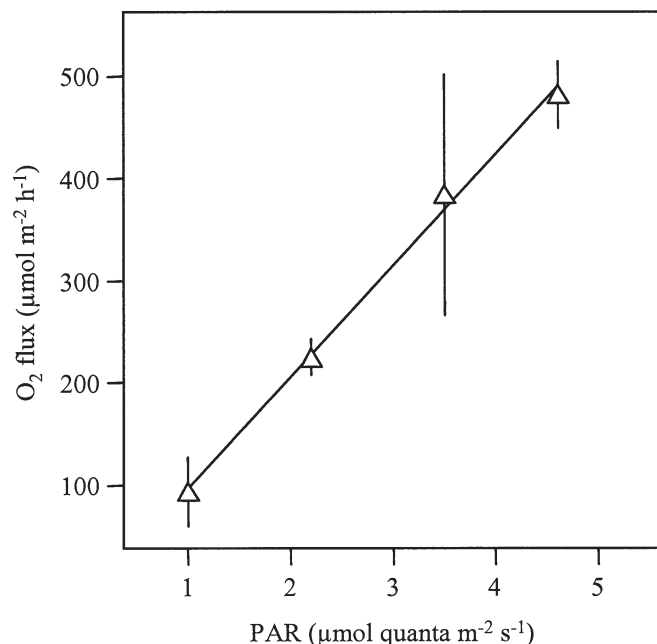


Fig. 4. Relationship between diffusive flux of O_2 across the mat–water interface and PAR. Linear fit, $R^2 = 0.9967$.

Depth-integrated net O_2 production in the upper 21 mm of a mat at 16.6-m water depth was $120 \mu\text{mol m}^{-2} \text{h}^{-1}$ under conditions of irradiance of PAR of $1 \mu\text{mol quanta m}^{-2} \text{s}^{-1}$. The flux of O_2 across the DBL was similar, $118 \mu\text{mol m}^{-2} \text{h}^{-1}$. There were four distinct zones of depth-integrated net O_2 production/consumption in the upper 21-mm-thick layer (Fig. 5B). Net O_2 production in the first 1.6-mm-thick layer was $117 \mu\text{mol m}^{-2} \text{h}^{-1}$; the underlying 3.4-mm-thick layer produced $11 \mu\text{mol O}_2 \text{m}^{-2} \text{h}^{-1}$. Note that, in contrast to the profile measured at 8.1-m water depth, the O_2 consumption profile shown in Fig. 5B describes a large fraction of the laminated, non-pigmented base of the mat. O_2 consumption in the non-pigmented zone of the mat was $4.1 \mu\text{mol m}^{-2} \text{h}^{-1}$ at depths between 5 mm and 6.6 mm and below 6.6 mm, was $3.6 \mu\text{mol m}^{-2} \text{h}^{-1}$.

Pinnacle mats—Densely spaced valleys, holes, and ridges at scales ranging from millimeters to centimeters structured the surface of pinnacle mats at 12-m water depth (Fig. 1B). Our chlorophyll fluorescence images indicate high concentration of chlorophyll along edges of pinnacles and, in some cases, at the very tips (Fig. 6A). Vertical $[O_2]$ profiles measured from a position above the mat into the valleys revealed steep gradients within the mat boundary and two characteristic peaks (Fig. 6B,C). The bottom water above the mat was O_2 oversaturated; concentrations ranged between $1.3 \text{ mmol O}_2 \text{L}^{-1}$ and $1.6 \text{ mmol O}_2 \text{L}^{-1}$ (285–350% saturation). $[O_2]$ peaked in the water surrounding the pinnacle tips, decreased rapidly towards the surface of the mat, and then increased again within the mat matrix.

RLC and rETR—Mats from 8.1-m water depth comprised a pigmented gelatinous matrix (20–25-mm thick) of

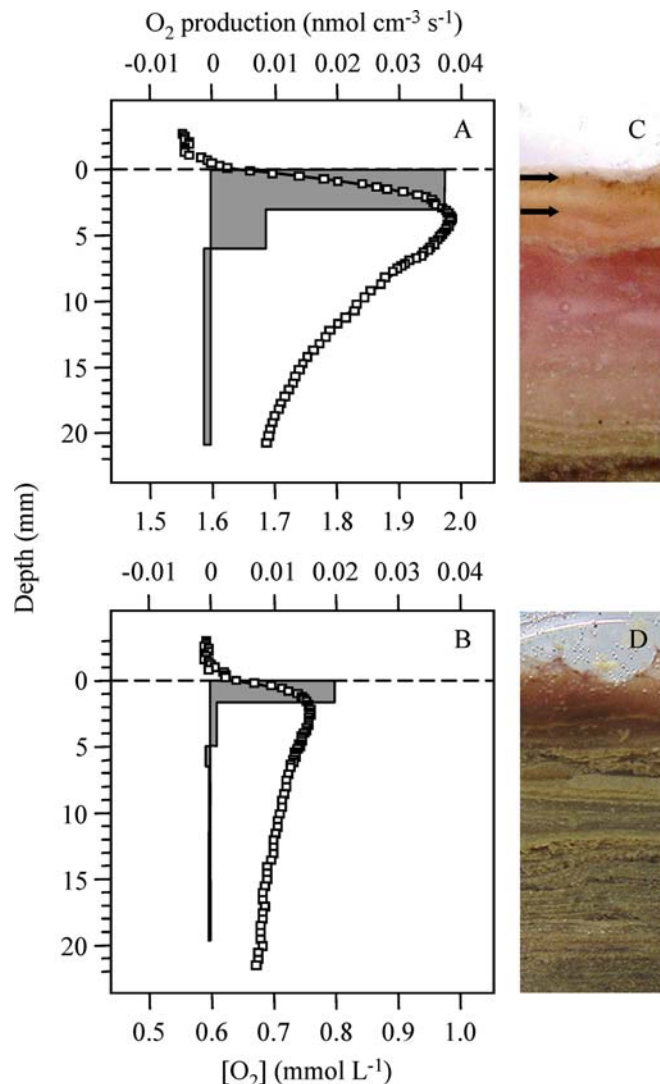
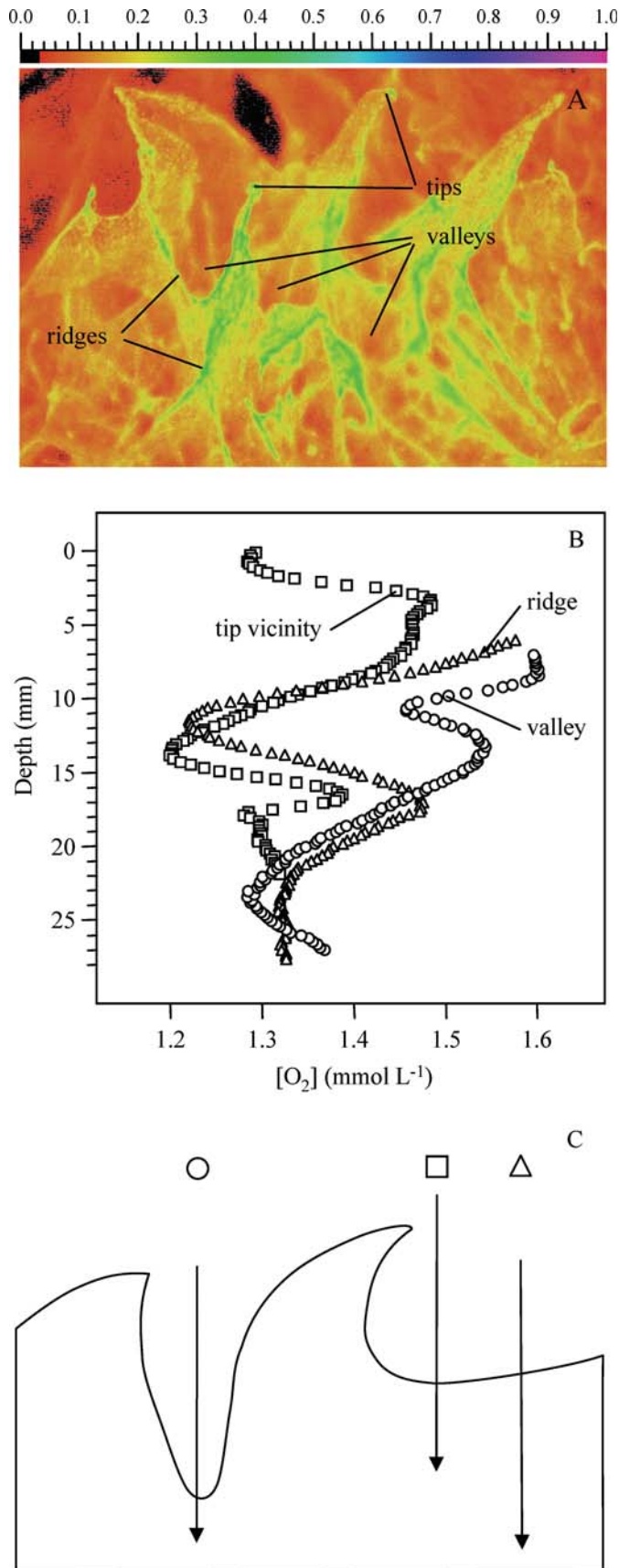


Fig. 5. (A, B) Two vertical in situ $[O_2]$ profiles (squares, lower scales) measured across mats at (A) 8.1-m and (B) 16.6-m water depth. At the time, irradiance was $4.6 \mu\text{mol quanta m}^{-2} \text{s}^{-1}$ and $1.0 \mu\text{mol quanta m}^{-2} \text{s}^{-1}$. The fits indicate the calculated best-fitting concentration profile (lower scale) and the bars indicate the connected net O_2 production profile (upper scales). R^2 for the best-fitting concentration profiles in (A) and (B) were 0.9990 and 0.9943, respectively. The dashed lines indicate the surface of the mats. The equilibrium atmospheric solubility for O_2 was $0.457 \text{ mmol L}^{-1}$. (C, D) Digital photographs of cross sections of mats from (A) 8.1-m and (B) 16.4-m water depth. Horizontal arrows on panel (C) indicate the location of the two most recent growth layers.

alternating optically dense (<1 mm thick) and hyaline (2–3-mm thick) layers overlying a base (several centimeter thick) composed of 0.5–1-mm-thick alternating bands of organic material and sand (Fig. 7C). The pigmented matrix consisted of an uppermost brownish layer (5-mm thick) followed by a pink layer and contained numerous sand grains and calcite crystals. In contrast to mats from 8.1-m water depth, the upper pigmented gelatinous matrix of mats from 16.6-m water depth was only 3–5-mm thick and



alternating optically dense and hyaline layers were ~ 1 -mm thick.

The two vertical panels in Fig. 7 illustrate the contrasting thickness of the chlorophyll-containing layer and the lamination of these layers at two depths. They show the same field of view of cross sections of mats from 8.1 m and 16.6 m, imaged with the PAM (as F_0 and as ϕ_p) and with a digital camera. Inspection of the F_0 images (Fig. 7A,D) revealed three laminae of pigments in the upper layer of the mats from 16.6-m water depth, but at least six laminae in the pigmented layer of mats from 8.1-m water depth. Chlorophyll fluorescence was maximal in the upper laminae of the mat from 8.1-m water depth and, with increasing depth into the mat, the chlorophyll fluorescence was associated with the optically dense layers. Inspection of the false color images of ϕ_p in Fig. 7B,E revealed little structure to this parameter.

Our two profiling PAM measurements across the cross sections of the upper pigmented layer of mats from 12-m water depth yielded similar values of all photosynthetic parameters, and showed a similar decline in E_k and $rETR_{max}$ with increasing depth into the mat (Table 3).

Discussion

We have demonstrated, for the first time, in situ benthic photosynthesis in a permanently ice-covered lake of the McMurdo Dry Valleys. We showed that microbial mats in Lake Hoare to at least 16.6-m water depth are net producers of O_2 during the summer period. To estimate the rates of O_2 evolution from in situ, steady-state $[O_2]$ profiles we used two different approaches: we calculated the efflux of O_2 across the DBL from the $[O_2]$ gradient in the DBL, and we used $[O_2]$ profiles in the upper 21-mm-thick layer of the mat to model the net O_2 production rate profile (Fig. 5) and the area-specific depth-integrated net O_2 production. It should be noted that the net O_2 production rate profiles were calculated assuming ϕ and D_s to be depth invariant, which may not be the case given the laminated structure of the mats, and that microelectrodes can affect the DBL when introduced from above and, thereby, the derived solute exchange rates (Glud et al. 1994). Furthermore, the calculation of net O_2 production rates and area-specific depth-integrated net O_2 production only includes the metabolic activity within the upper 21 mm of the mats, whereas estimates of the O_2 flux from the concentration profiles in the DBL integrate the total benthic activity, including O_2 consumption in the deeper (>21 mm depth) laminated sediment. General agreement

←

Fig. 6. (A) Chlorophyll fluorescence image showing the concentration of pigments associated with the small pinnacles (1–2 cm high) in the center of the picture. The false-color image shows low concentrations as red and higher concentrations as yellow, then green. (B) Three $[O_2]$ profiles across the surface of a pinnacle mat taken from 12-m water depth. (C) Sketch showing an outline of a section of a pinnacle mat and the approximate path of the microelectrode during measurements of the profiles shown in (B). Note the sketch is not in scale.

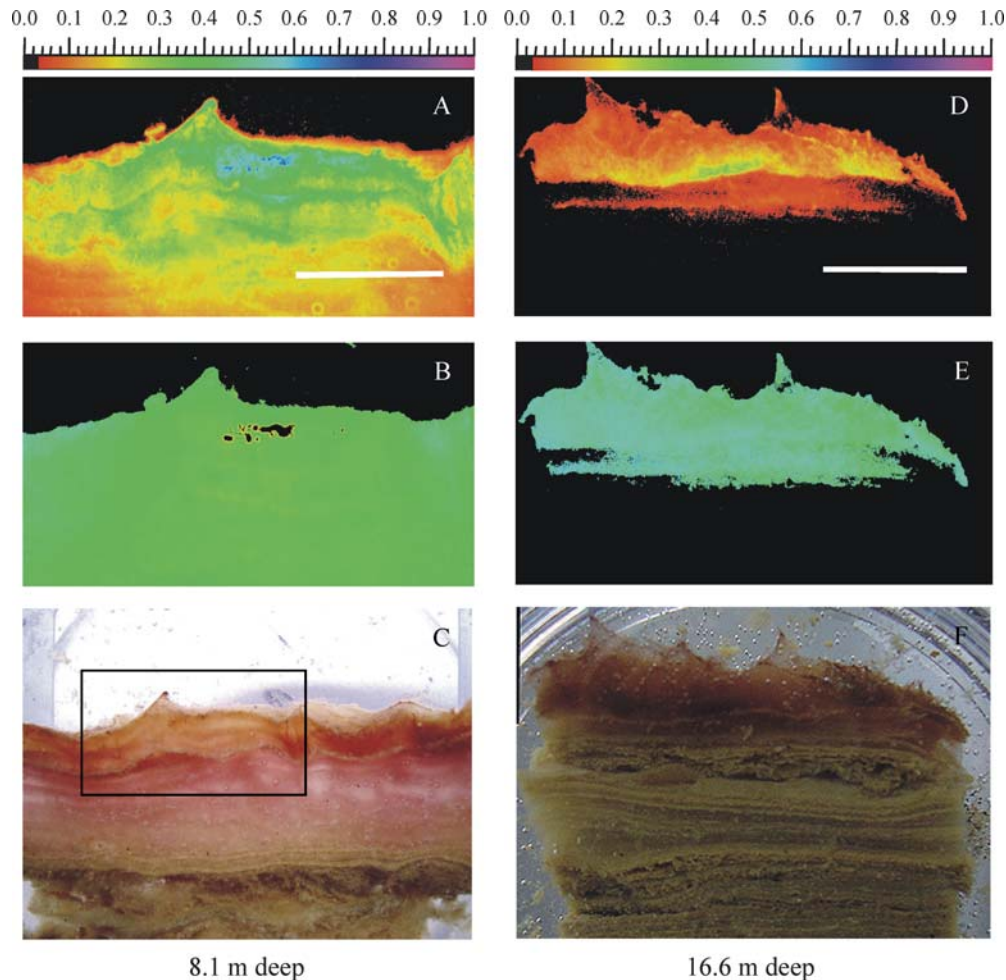


Fig. 7. Representative images of (A, D) the minimal fluorescence, F_0 , and (B, E) maximal photochemical yield, $(F_m - F_0) \times F_m^{-1}$, and (C, F) digital photograph of cross sections of the photosynthetic active zones. (A, B, C) Mat from 8.1-m water depth; (D, E, F) mat from 16.6-m water depth. The color-gradient scale indicates the magnitude of the fluorescence signal. Bar, 10 mm.

between the two estimates, however, indicates that the respiration in the deeper unpigmented laminated zone of the mat must be negligible. The production profile in Fig. 5B, which covers the upper part of the laminated unpigmented zone of the mat, actually indicates a very low volume specific consumption (respiration) of $7.61 \times 10^{-5} \text{ nmol O}_2 \text{ cm}^{-3} \text{ s}^{-1}$ at depths below 6.6 mm. Assuming a 10-cm-thick column of unpigmented laminated sediment, the area specific consumption in this zone would be $27.69 \mu\text{mol m}^{-2} \text{ h}^{-1}$ ($= 0.089 \mu\text{g cm}^{-2} \text{ h}^{-1}$), which is more than three times lower than the rates estimated for mats in Lake Hoare by Hawes and Schwarz (2000) based on the laboratory gas-exchange measurements. Such low decomposition rates, in combination with the lack of grazing and bioturbation by metazoans, the lack of strong internal currents, the continuous influx of sediment through the ice cover, and the accumulation of carbonates, may promote the formation and preservation of modern stromatolites that will eventually become lithified, resulting in lacustrine carbonate sedimentary deposits. This process may contribute significantly to water-column O_2 supersaturation because it isolates fixed carbon from the lake's

metabolism. Additional sources of O_2 may come from microbial mats that leave Lake Hoare after freezing into the ice cover (lift-off mats) and meltstreams carrying O_2 into this lake that is exsolved when water freezes onto the bottom of the ice cover (Wharton et al. 1986).

For mats from 7-m and 10-m water depth in Lake Hoare, Hawes et al. (2001) estimated rates of irradiance-saturated gross photosynthesis of $2.32 \mu\text{g O}_2 \text{ cm}^{-2} \text{ h}^{-1}$ and $2.06 \mu\text{g O}_2 \text{ cm}^{-2} \text{ h}^{-1}$ and maximum respiration rates of $0.58 \mu\text{g O}_2 \text{ cm}^{-2} \text{ h}^{-1}$ and $0.34 \mu\text{g O}_2 \text{ cm}^{-2} \text{ h}^{-1}$, respectively. Hence irradiance-saturated net photosynthesis would be $1.74 \mu\text{g O}_2 \text{ cm}^{-2} \text{ h}^{-1}$ and $1.72 \mu\text{g O}_2 \text{ cm}^{-2} \text{ h}^{-1}$, which translates to $543.8 \mu\text{mol O}_2 \text{ m}^{-2} \text{ h}^{-1}$ and $537.5 \mu\text{mol O}_2 \text{ m}^{-2} \text{ h}^{-1}$. These rates are 22–23% higher than the O_2 flux calculated from our in-situ measurements at 8.1-m water depth. This suggests that benthic photosynthesis was light-limited, and this was supported by our profiling RLC measurements. Phototrophs throughout the pigmented layer of the mat were photosynthetically competent, with E_k values that indicated that, at all irradiances likely to be experienced under ice, photosynthesis at all depths in the mat was light-limited, therefore operating at or close to

Table 3. Photosynthetic parameters estimated from RLC measurements using cross sections of mats from 8-m, 12-m, and 16-m water depth. E_k ($\mu\text{mol m}^{-2} \text{s}^{-1}$); rETR_{max} , ($\mu\text{mol electrons m}^{-2} \text{s}^{-1}$); α , ($[\text{mol electrons m}^{-2} \text{s}^{-1}] \times [\text{mol quanta m}^{-2} \text{s}^{-1}]^{-1}$); $(F_m - F_0) \times F_m^{-1}$, maximal photochemical yield.

Position	R^2	rETR_{max}	E_k	α	$(F_m - F_0) \times F_m^{-1}$
12 m A					
1	0.9962	14.23 \pm 0.36	28	0.507 \pm 0.012	0.569
2	0.9959	9.42 \pm 0.15	20	0.466 \pm 0.012	0.527
3	0.9920	8.00 \pm 0.18	20	0.389 \pm 0.014	0.485
4	0.9907	8.58 \pm 0.23	26	0.335 \pm 0.013	0.441
5	0.9924	7.48 \pm 0.17	23	0.322 \pm 0.011	0.427
6	0.9908	6.67 \pm 0.15	18	0.363 \pm 0.014	0.465
7	0.9821	5.60 \pm 0.16	15	0.381 \pm 0.020	0.503
12 m B					
1	0.9974	15.12 \pm 0.24	31	0.484 \pm 0.009	0.545
2	0.9968	12.18 \pm 0.19	25	0.470 \pm 0.011	0.530
3	0.9963	11.93 \pm 0.21	26	0.456 \pm 0.011	0.526
4	0.9953	11.54 \pm 0.34	34	0.343 \pm 0.009	0.438
5	0.9954	10.27 \pm 0.21	29	0.349 \pm 0.009	0.453
6	0.9932	8.90 \pm 0.19	23	0.384 \pm 0.012	0.502
7	0.9925	6.85 \pm 0.13	17	0.392 \pm 0.013	0.533

maximum quantum efficiency. Inferences on photoadaptive state from the RLC measurements are not definitive in this context. Given that the measurements were made on vertical sections of mat, with deeper mat layers exposed to non-ambient conditions, the estimates of E_k must be viewed with caution.

Our analysis of in situ $[\text{O}_2]$ profiles measured across mats at 16.6-m water depth lead to a similar conclusion of light limitation of photosynthesis. The depth-integrated net O_2 production was lower than the irradiance-saturated rates of net photosynthesis calculated by Hawes et al. (2001) for mats at 13-m and 19-m depth in Lake Hoare (375 $\mu\text{mol O}_2 \text{ m}^{-2} \text{ h}^{-1}$ and 116 $\mu\text{mol O}_2 \text{ m}^{-2} \text{ h}^{-1}$). We conclude that, in Lake Hoare, photosynthesis always occurs at or close to maximum efficiency, at all depths in the mat, and at all depths in the lake. That is, even minor changes in the intensity of the incident downwelling irradiance of PAR due to, for example, changes in the transparency of the ice cover or the optical properties of the water column (see, e.g., Howard-Williams et al. 1998) would significantly alter the rates of benthic carbon fixation.

The Imaging-PAM depictions of the minimal chlorophyll fluorescence yield, F_0 , and peaks in the profiles of attenuation of scalar irradiance within the mat indicate layering of the photosynthetic community. F_0 is, however, only a proxy for chlorophyll *a* and is affected by the efficiency of the light harvesting systems in intercepting and transferring energy within the various chlorophyll-containing organisms in microbial mats (Schreiber 2004). Banding of F_0 may indicate layering of those organisms that respond most to the excitation wavelengths used (diatoms, for example) rather than of the entire photosynthetic assemblage. Further support for layering of all phototrophs, however, is provided by the observation of bands within the mat where attenuation of diffuse irradiance in wavebands sensitive to both algal and cyanobacterial pigments increases proportionally more than that of the waveband

740–750 nm, where algal and cyanobacterial pigments show little absorbance. We note that bacteriochlorophylls absorb in the 740–750-nm waveband, but authors' unpublished analyses of mat pigments using high-performance liquid chromatography have detected bacteriochlorophylls only below 23-m water depth. Absorption in the 740–750-nm waveband can therefore be attributed primarily to non-pigmented materials such as sediment and organic debris. In contrast, attenuation of scalar irradiance at wavelengths of 575–585 nm, 625–635 nm, and 670–680 nm will include contributions from chlorophyll, phycoerythrin, and phycocyanin of diatoms and cyanobacteria. We found maxima in the attenuation coefficient of these wavebands at the same depths of 0–0.5 mm and 4 mm, coincident with maxima in F_0 (Fig 7A) and with the position of dense portions of the photograph in Fig. 5C (arrows). Note that our optical sensor had a relatively low spatial resolution, so the attenuating layers were only distinguishable in the uppermost zone of the mat where the thickness of the most recent annual layers was large enough. Layers at greater depths were compacted, and the spatial resolution of the sensor was too low to detect small-scale changes in attenuation.

The alternation between 5 months of growth and 7 months of no growth perhaps explains the origin of the horizontal alternating layers of hyaline and dense material in mats of Lake Hoare (Hawes et al. 2001). Hyaline layers apparently form during summer growth, while as growth slows in late summer, sedimentary material, which enters this lake during late summer meltwater flow and through cracks in ice cover (Priscu et al. 1999), may settle on the mat surface. Optically dense layers form in winter when photosynthesis and growth stop, and the phototrophs and sediments accumulate at the surface. With the onset of daylight, renewed growth of surviving trichomes initiates a new hyaline layer. Trichomes that survive but do not grow vertically may remain as the horizontal layer in a way

analogous to that described by Doemel and Brock (1977) for warm-water laminated mats.

Hawes et al. (2001) estimated that the growth of mats in Lake Hoare at water depth between 7 m and 19 m results in an annual increase in mat thickness between 2.5 mm and 0.2 mm. Consequently, the uppermost zone of high net photosynthesis shown in Fig. 5A,B (bars) likely constituted the recent (2004) annual layer, whereas photosynthesis in the underlying zone would have been caused by the activity of the previous-year layers. Hence, photosynthesis, and potentially therefore growth, in mats from 8–16-m water depth may not be confined to the most recent annual layer. The images in Fig. 7B,E revealed no vertical structure to the parameter ϕ_p , which indicates that all of the fluorescing chlorophyll in the previous-year layers was connected to fully competent photosystems. As discussed above, slicing the mat vertically and exposing the cross section to air-saturated water will have altered conditions for photosynthesis, and while these images do indicate the potential for high efficiency in the deeper mat layers, they do not show this to occur in situ. Another experimental uncertainty is the fact that the operational depth/volume from which fluorescence signals are obtained rely on the optical density of the mat. During the saturation, pulse fluorescence from deeper layers can contribute to the signal, while measurements of F -values, especially at low actinic irradiances, sample from shallower layers. Thus, yield measurements represent averages over an unknown volume, which can lead to artifacts (see e.g., Grunwald and Kühl 2004).

Assuming a molar ratio of C : O = 1.2 : 1 and that the absorption efficiency is the same for pigment arrays at different water depths, we used the slope of our irradiance-versus- O_2 -flux curve (Fig. 4) to estimate an area-specific maximum community quantum yield of 0.073 mol carbon (C) per mol photons incident to the mat surface (1 mol of carbon fixed for every 13.7 mol incident photons). This yield is similar to that calculated by Hawes and Schwarz (1999) for mats from 10-m water depth in Lake Hoare: 0.06 mol C mol⁻¹ quanta. (Our calculation still underestimates the actual yield because we do not partition photon absorption between pigments and other matter.) Extrapolation of the irradiance-versus- O_2 -flux curve in Fig. 4 revealed a low compensation irradiance of 0.1 μ mol quanta m⁻² s⁻¹, reflecting high shade acclimation. Again, this result supports the low compensation-irradiance estimates of <0.5 μ mol quanta m⁻² s⁻¹ for mats in Lake Hoare from >13-m water depth published by Hawes and Schwarz (1999, 2000).

Our measurements within the boundary of pinnacle mats revealed a complex small-scale chemical landscape. These measurements and the images in Figs. 1B and 6A indicate that a one-dimensional approach to quantification of solute exchange and reaction rates may not be a good approximation for this type of mat (see also Jørgensen and Des Marais 1990, and Glud et al. 1999). We selected areas devoid of pinnacles for measuring in situ O_2 profiles (e.g., see Fig. 1A) and this methodological necessity may have resulted in an underestimation of areal production in heavily pinnacled areas. The origin and function of the pinnacles in such pinnacle mats is unknown, but may be

caused by positive phototaxis similar to that reported on pinnacle mats in hot springs (Walter 1977). However, the formation of pinnacles does not automatically imply photomovement. In many low-flow or stagnant environments, mats with pinnacle structures develop. This can in some cases be due to formation of internal gas bubbles that are overgrown and in other cases be a strategy to overcome or minimize diffusion limitation of solute exchange. Also, largely non-motile mats in other environments can develop conspicuous pinnacles over time (Kühl et al. 2003).

In conclusion, we have shown that microbial mats in Lake Hoare to at least 16.6-m water depth are net producers of O_2 during the summer period. We confirmed key parameters of benthic photosynthesis previously derived only from laboratory gas-exchange measurements, and we present evidence that photosynthesis in the mats occurs, at all depths in the mat and at all lake depths, at or close to maximum photosynthetic efficiency. This simplifies modeling simulations of benthic photosynthesis in the lake, and implies that annual production will be related to ice and water transparency, which vary from year to year (Howard-Williams et al. 1998). Our high-resolution laboratory measurements at the surface of pinnacle mats revealed a complex small-scale chemical structure of the mat–water interface. We propose manipulative in-situ experiments to understand the mechanisms that lead to the formation of pinnacles and to reveal the implications of such structures for light-limited growth in the diffusion-dominated permanently ice-covered lakes.

References

- BERG, P., N. RISGAARD-PETERSEN, AND S. RYSGAARD. 1998. Interpretation of measured concentration profiles in sediment pore water. *Limnol. Oceanogr.* **43**: 1500–1510.
- BROECKER, W. S., AND T.-H. PENG. 1974. Gas exchange rates between air and sea. *Tellus* **26**: 185–190.
- CATHEY, D. D., B. C. PARKER, G. M. SIMMONS, W. H. YONGUE, AND M. R. VAN BRUNT. 1981. The microfauna of algal mats and artificial substrates in Southern Victoria Land lakes of Antarctica. *Hydrobiologia* **85**: 3–15.
- CRAIG, H., R. A. WHARTON, JR., AND C. P. MCKAY. 1992. Oxygen supersaturation in ice-covered Antarctic lakes: Biological versus physical contributions. *Science* **255**: 318–321.
- DOEMEL, W. N., AND T. D. BROCK. 1977. Structure, growth, and decomposition of laminated algal-bacterial mats in alkaline hot springs. *Appl. Environ. Microbiol.* **34**: 433–452.
- DORAN, P. T., C. P. MCKAY, G. D. CLOW, G. L. DANA, A. G. FOUNTAIN, T. NYLEN, AND W. B. LYONS. 2002a. Valley floor climate observations from the McMurdo dry valleys, Antarctica, 1986–2000. *J. Geophys. Res.* **107**: 4772.
- , AND OTHERS. 2002b. Recent climate cooling and ecosystem response in the McMurdo Dry Valleys, Antarctica. *Nature* **415**: 517–520.
- DORE, J. E., AND J. C. PRISCU. 2001. Phytoplankton phosphorus deficiency and alkaline phosphatase activity in the McMurdo Dry Valley lakes, Antarctica. *Limnol. Oceanogr.* **46**: 1331–1346.
- EPPING, E. H. G., A. KHALILI, AND R. THAR. 1999. Photosynthesis and the dynamics of oxygen consumption in a microbial mat as calculated from transient oxygen microprofiles. *Limnol. Oceanogr.* **44**: 1936–1948.

- GLUD, N. G., J. K. GUNDERSEN, N. P. REVSBECH, AND B. B. JØRGENSEN. 1994. Effects on the benthic diffusive boundary layer imposed by microelectrodes. *Limnol. Oceanogr.* **39**: 462–467.
- , M. KÜHL, O. KOHLS, AND N. B. RAMSING. 1999. Heterogeneity of oxygen production and consumption in a photosynthetic microbial mat as studied by planar optodes. *J. Phycol.* **35**: 270–279.
- GRUNWALD, B., AND M. KÜHL. 2004. A system for imaging variable chlorophyll fluorescence of aquatic phototrophs. *Ophelia* **58**: 79–89.
- HAWES, I., D. MOORHEAD, D. SUTHERLAND, J. SCHMELING, AND A.-M. SCHWARZ. 2001. Benthic primary production in two perennially ice-covered Antarctic lakes: patterns of biomass accumulation with a model of community metabolism. *Antarctic Science* **13**: 18–27.
- , AND A.-M. SCHWARZ. 1999. Photosynthesis in an extreme shade environment: benthic microbial mats from Lake Hoare, a permanently ice-covered Antarctic lake. *J. Phycol.* **35**: 448–459.
- , AND ———. 2000. Absorption and utilization of irradiance by cyanobacterial mats in two ice-covered Antarctic lakes with contrasting light climates. *J. Phycol.* **37**: 5–15.
- , D. SUTHERLAND, AND D. HANELT. 2003. The use of pulse amplitude modulated fluorometry to determine fine-scale temporal and spatial variation of in situ photosynthetic activity within an *Isoetes*-dominated canopy. *Aquat. Bot.* **77**: 1–15.
- HEYWOOD, R. B. 1984. Antarctic inland waters, p. 279–344. *In* R. M. Laws [ed.], *Antarctic ecology*, v. 1. Academic.
- HOFSTRAAT, J. W., J. C. H. PEETERS, J. F. H. SNEL, AND C. GEEL. 1994. Simple determination of photosynthetic efficiency and photoinhibition of *Dunaliella tertiolecta* by saturating pulse fluorescence measurements. *Mar. Ecol. Prog. Ser.* **103**: 187–196.
- HOWARD-WILLIAMS, C., A.-M. SCHWARZ, AND I. HAWES. 1998. Optical properties of the McMurdo Dry Valley Lakes, Antarctica. *Antarctic Research Series* **72**: 189–203.
- JASSBY, A. D., AND T. PLATT. 1976. Mathematical formulation of the relationship between photosynthesis and light for phytoplankton. *Limnol. Oceanogr.* **21**: 540–547.
- JØRGENSEN, B. B., AND D. J. DES MARAIS. 1990. The diffusive boundary layer of sediments: Oxygen microgradients over a microbial mat. *Limnol. Oceanogr.* **35**: 1343–55.
- KIRK, J. T. O. 1983. *Light and photosynthesis in aquatic ecosystems*. Cambridge.
- KÜHL, M., T. FENCHEL, AND J. KAZMIERCZAK. 2003. Growth, structure and calcification potential of an artificial cyanobacterial mat, p. 77–102. *In* W. E. Krumbein, D. Paterson, and G. Zavarzin [eds.], *Fossil and recent biofilms, a natural history of life on Earth*. Kluwer.
- , R. N. GLUD, J. BORUM, R. ROBERTS, AND S. RYSGAARD. 2001. Photosynthetic performance of surface-associated algae below sea ice measured with a pulse-amplitude-modulated (PAM) fluorometer and O₂ microsensors. *Mar. Ecol. Prog. Ser.* **223**: 1–14.
- LASSEN, C., PLOUGH, AND B. B. JØRGENSEN. 1992. A fiber-optic scalar irradiance microsensor: Application for spectral light measurements in sediments. *FEMS Microbial Ecol.* **86**: 247–254.
- LI, Y.-H., AND S. GREGORY. 1974. Diffusion of ions in sea water and in deep-sea sediments. *Geochim. Cosmochim. Acta* **38**: 703–714.
- LIZOTTE, M. P., AND J. C. PRISCU. 1992. Photosynthesis-irradiance relationship from the physically stable water column of a perennially ice-covered lake (Lake Bonney, Antarctica). *J. Phycol.* **28**: 179–185.
- MOORHEAD, D., J. SCHMELING, AND I. HAWES. 2005. Modeling the contribution of benthic microbial mats to net primary production in Lake Hoare, McMurdo Dry Valleys. *Antarctic Science* **17**: 33–45.
- PARKER, B. C., G. M. SIMMONS, JR., F. G. LOVE, R. A. WHARTON, JR., AND K. G. SEABURG. 1981. Modern stromatolites in Antarctic dry valley lakes. *BioScience* **31**: 656–661.
- PRISCU, J. C., L. R. PRISCU, W. F. VINCENT, AND C. HOWARD-WILLIAMS. 1987. Photosynthate distribution by microplankton in permanently ice-covered Antarctic desert lakes. *Limnol. Oceanogr.* **32**: 260–270.
- , AND OTHERS. 1999. Carbon transformations in a perennially ice-covered Antarctic lake. *BioScience* **49**: 997–1007.
- RALPH, P. J., AND R. GADEMANN. 2005. Rapid light curves: A powerful tool to assess photosynthetic activity. *Aquat. Bot.* **82**: 222–237.
- , U. SCHREIBER, R. GADEMANN, M. KÜHL, AND A. D. W. LARKUM. 2005. Coral photobiology studied with a new imaging pulse amplitude modulated fluorometer. *J. Phycol.* **41**: 335–342.
- REVSBECH, N. P. 1989. An oxygen microelectrode with a guard cathode. *Limnol. Oceanogr.* **34**: 474–478.
- SCHREIBER, U. 2004. Pulse-amplitude (PAM) fluorometry and saturation pulse method, p. 279–319. *In* G. Papageorgiou and Govindjee [eds.], *Chlorophyll fluorescence: A signature of photosynthesis*. Advances in photosynthesis and respiration series, Kluwer.
- , M. KÜHL, I. KLIMANT, AND H. REISING. 1996. Measurement of chlorophyll fluorescence within leaves using a modified PAM fluorometer with a fiber-optic microprobe. *Photosynth. Res.* **47**: 103–109.
- VINCENT, W. F. 1981. Production strategies in Antarctic inland waters: Phytoplankton eco-physiology in a permanently ice-covered lake. *Ecology* **62**: 1215–1224.
- WALTER, M. R. 1977. Interpreting stromatolites. *American Scientist* **65**: 563–571.
- WHARTON, JR., R. A., W. B. LYONS, AND D. J. DES MARAIS. 1993. Stable isotopic biogeochemistry of carbon and nitrogen in a perennially ice-covered Antarctic lake. *Chemical Geology (Isotope Geoscience Section)* **107**: 159–172.
- , C. P. MCKAY, G. M. SIMMONS, JR., AND B. C. PARKER. 1986. Oxygen budget of a perennially ice-covered Antarctic lake. *Limnol. Oceanogr.* **31**: 437–443.
- , M. A. MEYER, C. P. MCKAY, R. L. MANCINELLI, AND G. M. SIMMONS, JR. 1994. Sediment oxygen profiles in a super-oxygenated Antarctic lake. *Limnol. Oceanogr.* **39**: 839–853.
- , B. C. PARKER, AND G. M. SIMMONS, JR. 1983. Distribution, species composition and morphology of algal mats in Antarctic dry valley lakes. *Phycologia* **22**: 355–365.

Received: 13 October 2005
 Accepted: 23 February 2006
 Amended: 7 March 2006